Published in final edited form as:
Inorg Chem. 2009 August 3; 48(15): 7026–7032. doi:10.1021/ic801864z.

Multifrequency EPR Studies of $[Cu^{1.5}Cu^{1.5}]^{1+}$ for $Cu_2(\mu\text{-}NR_2)_2$ and $Cu_2(\mu\text{-}PR_2)_2$ Diamond Cores

Neal P. Mankad[ζ]
Department of Chemistry, Massachusetts Institute of Technology, Cambridge MA 02139

Seth B. Harkins[ℑ]
Department of Chemistry, California Institute of Technology, Pasadena CA 91125

William. E. Antholine[ξ]
Department of Biophysics, Medical College of Wisconsin, Milwaukee, Wisconsin 53226

Jonas C. Peters[ζ,*]
Department of Chemistry, Massachusetts Institute of Technology, Cambridge MA 02139

Abstract

Multifrequency EPR spectroscopy is used to explore the electronic structures of a series of dicopper complexes of the type the $\{(LXL)Cu\}_2^+$. These complexes contain two four-coordinate copper centers of highly distorted tetrahedral geometries linked by two $[LXL]^-$ ligands featuring bridging amido or phosphido ligands and associated thioether or phosphine chelate donors. Specific chelating $[LXL]^-$ ligands examined in this study include bis(2-*tert*-butylsulfanylphenyl)amide (SNS), bis(2-di-*iso*-butylphosphinophenyl)amide (PNP), and bis(2-di-*iso*-propylphosphinophenyl)phosphide (PPP). To better map the electronic coupling to copper, nitrogen, and phosphorus in these complexes, X-, S-, and Q-band EPR spectra have been obtained for each complex. The resulting EPR parameters implied by computer simulation are unusual for typical dicopper complexes and are largely consistent with previously published XAS and DFT data, where a highly covalent $\{Cu_2(\mu\text{-}XR_2)_2\}^+$ diamond core has been assigned in which removal of an electron from the neutral $\{Cu_2(\mu\text{-}XR_2)_2\}$ can be viewed as ligand centered to a substantial degree. To our knowledge, this is the first family of dicopper diamond core model complexes for which the compendium of X-, S-, and Q-band EPR spectra have been collected for comparison to Cu_A.

Keywords

EPR; Cu_A; mixed-valence; class III; redox-active ligands; dicopper; diamond core

Introduction

A long-standing subject of interest in the field of bioinorganic chemistry concerns the mode by which metalloenzymes mediate electron transfer (ET).[i,ii] This is especially true of enzymes that feature redox-active copper centers that serve as ET relays, such as the type 1 sites in blue copper proteins [iii,iv,v] and the Cu_A sites of cytochrome *c* oxidases and nitrous oxide reductases.

*Email: jcpeters@mit.edu.
[ζ]Massachusetts Institute of Technology
[ℑ]California Institute of Technology
[ξ]Medical College of Wisconsin

Supporting Information Available: Crystallographic data (cif) and supporting EPR spectra are available free of charge via the Internet at http://pubs.acs.org.

To mediate rapid ET, the local geometry of the copper center(s) must undergo rather little structural change during a redox event so as to minimize the reorganizational term λ,[vi] which when large serves to attenuate rates of ET. Therefore it is of particular interest to understand how copper centers achieve such low structural reorganization in proteins, and by analogy in small molecule model complexes.[vii,viii,ix,x] One hypothesis that has been widely advanced is that of the `entatic' or strained state, whereby it is presumed that in order to minimize λ a protein matrix confers a geometry at the redox active site that is similar to the transition state for the ET reaction, a geometry (and function) that would not be prevalent in the absence of the protein matrix. This hypothesis was first advanced by Vallee and Williams,[xi] and various researchers, most notably Rorabacher and coworkers,[xii] have sought small molecule model systems to explore the viability of this approach.

An alternative explanation as to how copper-containing enzymes mediate rapid ET concerns their intimate electronic structures, and the role that metal-ligand covalency plays in providing stabilized electronic states, as opposed to a geometrically strained state. Solomon and Ryde have been amongst those advancing this idea,[xiii] both in type 1 copper enzymes and also in Cu_A in which short and highly covalent Cu-S bonds are prevalent.

Efforts in our laboratories have focused on the preparation of small molecule model complexes that feature the $Cu_2(\mu XR_2)_2$ diamond core motif.[xiv xv,xvi,xvii] These complexes contain two four-coordinate copper centers of highly distorted tetrahedral geometries linked by two bridging XR_2^- ligands (where XR_2^- = NR_2^- or PR_2^-), where the R groups provide neutral donor groups (e.g., thioether or phosphine) to complete the copper coordination spheres. To date, the three systems shown in Figure 1 have been reported.[xiv,xvi,xv,xvii] A common feature of each of these systems is a fully reversible one-electron redox couple between the reduced dicopper (I,I) state and a one-electron oxidized fully delocalized mixed-valence dicopper(1.5,1.5) state. In this regard, each system is a good functional model of Cu_A. Indeed, the rate of electron self-exchange can be very rapid (> 10^7 M^{-1} s^{-1}), as has been estimated for the $\{(SNS)Cu\}_2$ system by NMR line-broadening analysis ((SNS) = bis(2-*tert*-butylsulfanylphenyl)amide; see Figure 1).[xiv] X-ray diffraction studies have established that the overall structural reorganization between each set of redox pairs is small. This is especially true of $Cu_2(\mu\text{-}NR_2)_2$ systems supported by the (SNS) and (PNP) ligands, where (PNP) represents the bis(2-di-*iso*-butlyphosphinophenyl)amide ligand.[xiv,xvii] In these cases, the most noteworthy structural change pertains to a Cu…Cu compression of ~ 0.15 Å upon one-electron oxidation. This compression is far more pronounced for the (PPP) system (> 0.5 Å),[xv] where (PPP) = bis(2-di-*iso*-propylphosphinophenyl)phosphide.

A recent comparative X-ray crystallographic, XAS, and DFT study of the series of compounds $\{(^t\text{Bu-PNP})Cu\}_2^{n+}$ and $\{(PPP)Cu\}_2^{n+}$ (where n = 0, 1, 2; ^{t}Bu-PNP = bis(2-di-*iso*-butlyphosphino-5-*tert*-butylphenyl)amide) sought to establish the role played by the bridging X and Cu atoms during successive oxidations. Based upon that study,[xvii] it was inferred that a substantial degree of ligand oxidation was prevalent. Indeed, a majority of oxidation occurs at the bridging diarylamido or diarylphosphido units compared with the copper centers, though there is appreciable copper d-character in the redox active molecular orbitals (RAMOs). What is very clear is that the $Cu_2(\mu\text{-}XR_2)_2$ diamond core is a highly covalent unit, and one cannot decouple the oxidation of the metal or bridging atoms from one another. This scenario is also true of the Cu_A site, where it has been estimated that the RAMO in the $Cu_2(\mu\text{-}SR)_2$ mixed-valence state is ~46% sulfur and ~44% copper.[xiii]

To more fully develop the electronic structure description of these redox active diamond core dicopper systems we undertook EPR studies of the $Cu^{1.5}Cu^{1.5}$ complexes. Whereas initial studies reported the X-band EPR spectra,[xiv,xv,xvi] a detailed analysis of the convoluted spectra had not been performed. To aid such an analysis, we have now collected comparative Q-, X-,

and S-band EPR spectra for each system shown in Figure 1. This set of data is unique for dicopper model systems, and allows for the possibility of quantifying hyperfine interactions between various centers and the unpaired spin, critical in describing their electronic structures and for comparison to published XAS and DFT studies, and related data available for Cu_A. Indeed, deconvolution of the EPR parameters by computer simulation reveals values unusual for typical dicopper systems and consistent with a large degree of Cu-XR_2 spin delocalization.

Experimental Section

Dicopper complexes were prepared according to previously published procedures[xiv,xv,xvi,xvii] as their $B[3,5\text{-}(F_3C)_2C_6H_3]_4$ salts and EPR spectra were recorded on frozen glasses in 2-methyltetrahydrofuran (5 mM). EPR spectra were obtained at the National Biomedical EPR Center in Milwaukee using Varian E-9 and E109 spectrometers operating at 9 GHz (X-band), 3.3 GHz (S-band) and 35 GHz (Q-band). The low frequency 3.3 GHz (S-band) spectrometer is based on the loop-gap resonator designed by Froncisz and Hyde.[xviii] The Q-band bridge was modified with the addition of a GaAs field-effect transistor signal amplifier and low-noise Gunn diode oscillator.[xix] Microwave frequencies were measured with an EIP model 331 counter. Simulations were carried out using the program Xsophe (Bruker). Xsophe simulations were calculated using matrix diagonalization. Unless otherwise indicated, simulations assumed hyperfine interactions of the unpaired electron with 2 equivalent Cu atoms, 2 equivalent bridging (N or P) atoms, and 2 equivalent non-bridging P atoms where available (*vide infra*).

Spectrometer conditions were as follows. Q-band: microwave power 36 dB, temperature 16.7K, mod. amplitude 5G set [actual about 3 G], time constant 0.1 sec, 100 KHz mod. frequency, scan time 4 min., microwave frequencies 35.011 GHz (PPP), 35.0008 GHz (SNS), 35.028 GHz (PNP). S-band: microwave power 22 dB, temperature -140 °C, mod. amplitude 5 set [actual about 3 G], time constant 0.064 sec, scan time 2 min., microwave frequencies 3.3661 GHz (SNS), 3.3642 GHz (PNP); PPP 3.3416 GHz (PPP). X-band: microwave power 16 dB, temperature 120 K, mod. amplitude 5 G, time constant 0.128 sec, scan time 4 min., microwave frequencies 9.434 GHz (PPP), 9.431 GHz (PNP), 9.457 GHz (SNS).

Results

X- and Q-band EPR spectra of $\{(PPP)Cu\}_2^+$, $\{(PNP)Cu\}_2^+$, and $\{(SNS)Cu\}_2^+$

X-band EPR spectra for the mixed valence compounds $\{(PPP)Cu\}_2^+$,[xv], $\{(PNP)Cu\}_2^+$,[xvi] and $\{(SNS)Cu\}_2^+$,[xiv] are similar to spectra recorded previously (Figure 2, Table 1).[xx] The *g*-values are more apparent from the Q-band (35 GHz) spectra (Figure 3, Table 1). The g_{min} values determined from Q-band can then be used for X-band simulations. The hyperfinefine structure in the Q-band spectrum for $\{(PPP)Cu\}_2^+$ is still resolved indicating that there is little *g*-strain. Neither g_{max} nor g_{min} is separated from the center *g*-value for $\{(PPP)Cu\}_2^+$, consistent with an isotropic *g*-value at this resolution. A high field line for g_{min} in the Q-band spectra for $\{(PNP)Cu\}_2^+$ and $\{(SNS)Cu\}_2^+$ is separated (Figure 3). This high field *g*-value is apparent in the X-band spectrum for $\{(SNS)Cu\}_2^+$, but not as apparent for $\{(PNP)Cu\}_2^+$ or $\{(PPP)Cu\}^+_2$ (Figure 2). The hyperfine structure is not resolved in the Q-band spectra for $\{(PNP)Cu\}_2^+$ and $\{(SNS)Cu\}_2^+$ where *g*-strain contributes to the broadening of the lines.

S-band spectra of $\{(PPP)Cu\}_2^+$, $\{(PNP)Cu\}_2^+$, and $\{(SNS)Cu\}_2^+$

The hyperfine structure in the spectra for $\{(PPP)Cu\}^+_2$, $\{(PNP)Cu\}_2^+$, and $\{(SNS)Cu\}_2^+$ is better resolved in the low frequency S-band spectra (Figure 4). Additional lines in the S-band spectrum for $\{(PNP)Cu\}_2^+$ are resolved on the high field side where there are only inflections in the X-band spectrum (Figure 2). The *g*-value close to the crossover point in Figure 4 is

g_{iso} for $\{(PPP)Cu\}_2^+$ and is close to g for $\{(PNP)Cu\}_2^+$ and $\{(SNS)Cu\}_2^+$ as taken from the Q-band data. The g-anisotropy is not as evident at S-band because the g-values are getting closer as determined by field position. Using the g-value determined for $\{(SNS)Cu\}_2^+$ and $\{(PNP)Cu\}_2^+$ at Q-band, g_{mid} is determined in the center of the spectrum. Equally spaced lines around g_{mid} are the hyperfine lines. There should be a 1:2:3:4:3:2:1 seven line pattern centered at g_{mid} if the hyperfine lines are only from two coppers. The observed eleven lines are consistent with a 1:4:10:20:26:28:26:20:10:4:1 pattern for $\{Cu_2(\mu\text{-}NR_2)_2\}^+$ where the hyperfine couplings are about equal for copper and nitrogen (Figs 2 and 4).

Second derivative multifrequency EPR spectra and simulations for $\{(PPP)Cu\}_2^+$

The second derivative of an EPR spectrum emphasizes sharp lines and deemphasizes broad lines. Of the three complexes described in this paper, the hyperfine lines for $\{(PPP)Cu\}_2^+$ are most apparent and easiest to compare at X-, Q-, and S-band frequencies (Figure 5). The spectra are centered at the apparent, to first order, isotropic g-value, 2.003. The large number of resolved lines in the X- and S-band spectra of each species, most apparent in the second derivative spectrum for $\{(PPP)Cu\}_2^+$ in Fig. 5, suggests that the hyperfine lines are not from only copper. Two almost equivalent coppers in $\{(PPP)Cu\}_2^+$ are expected to give seven lines for each g-value. If the lines are from more than one g-value, they should not line up at three different microwave frequencies. About twenty lines are almost aligned at the three frequencies. This indicates that the hyperfine lines are due to not only Cu (I = 3/2), but also P (I = 1/2) assuming that the copper hyperfine lines are from equivalent coppers and not inequivalent coppers with different hyperfine values. The lines are better resolved as the frequency is lowered. Moreover, almost all of the hyperfine lines line up at all three frequencies. At the higher frequencies, the relative intensities are not evident due to line broadening and partial overlap of the lines. At S-band, the lines are so well resolved that the relative intensity of the lines becomes more evident. For example, on the low field side of the spectrum, some of the lines have relative intensities of 1:2:1 consistent with coupling to two almost equivalent nuclei with I = 1/2, i.e. a pattern due to two almost equivalent P atoms (Figure 5, circled area). Assigning the 1:2:1 pattern to two almost equivalent P atoms gives $A^{P(terminal)}$ = 12.5 G. The next three lines also form a 1:2:1 pattern. The difference in field for the centers of both 1:2:1 patterns gives a second hyperfine value assigned to copper and phosphorous, i.e. $A^{Cu} \sim A^{P(bridge)}$ = 45 G. Note that a 1:4:6:4:1 pattern is expected for four equivalent P atoms, and it is difficult to distinguish between a 1:2:1 and a 4:6:4 pattern where the lines with intensity 1 are superimposed onto more intense lines. It is also possible that geometric factors dictate inequivalent coupling of the unpaired spin to the terminal phosphines, much like coupling that is observed with the CH_2 protons in the tyrosine radical in ribonucleotide reductase.[xxi] Simulation of the spectra with A^{Cu} = 45 G, $A^{P(bridge)}$ = 45 G and $A^{P(terminal)}$ = 12.5 G and a line width of 5 G gives a multi-line pattern that is better resolved than the experimental S-band spectrum for $\{(PPP)Cu\}_2^+$ because the line width is less for the simulation than for the experimental spectrum (Supplemental Figure S1). The number of lines and the splitting of the lines in the simulation are similar to the lines in the experimental spectrum. A limitation of this simulation is that the variables are underdetermined. The g- and A-axes are taken as coincident with all Euler angles at zero. M_I-dependent line width parameters and quadruple terms were not used. The simulation is thus consistent with, but not proof of, the values for the experimental spectrum.

Second derivative EPR spectra and simulations for $\{(PNP)Cu\}_2^+$ and $\{(SNS)Cu\}_2^+$

The X-band spectrum for $\{(PNP)Cu\}_2^+$ (Figure 2) has ten clearly resolved lines in the center of the spectrum, which is attributed to the g_{mid} region. The resolved lines for $\{(PNP)Cu\}_2^+$ are broader than the lines for $\{(SNS)Cu\}_2^+$ presumably due to the superhyperfine lines from the terminal P-atoms. Initial simulation of a single isotropic line with a line width of 6 G and subsequent addition of hyperfine lines for two phosphorous atoms with $A^{P(terminal)}$ = 5 G

doubles the peak-to-peak width from 7 G to 15 G (data not shown). It is estimated that $A^{P(terminal)} \sim 5$ G from this simulation of the single line. If four phosphorous atoms are almost equivalent, $A^{P(terminal)}$ should be slightly less than 5 G. The second derivative of this spectrum emphasizes the lines that are resolved (Figure 6). Since only seven lines for the g_{mid} region are expected for the copper hyperfine from a class III mixed-valence complex, hyperfine lines from nitrogen were again considered to increase the number of lines. Simulation of the Q-band data, which is the most sensitive to *g*-values, provided the rhombic tensors g_{max}, g_{mid}, and g_{min} of 2.085, 2.060, and 2.000, respectively (Supplemental Figure S2). A good simulation of the X-band spectrum for $\{(PNP)Cu\}_2^+$ can be then obtained with g_{max}, g_{mid}, and g_{min} values of 2.085, 2.057, and 2.000; A^{Cu} values of 40, 27, and 15 G; and A^N values of 12, 24, and 15 G (Figure 6). The S-band spectrum may also be fit using these parameters (Supplemental Figure S3), lending weight to their assignments.

As already noted, the X-band EPR spectrum of $\{(SNS)Cu\}_2^+$ has been published and a crude simulation is consistent with the class III mixed-valence species.[xx] As for $\{(PPP)Cu\}_2^+$, second derivative spectra for $\{(SNS)Cu\}_2^+$ emphasize the sharp features in the spectra (Figure 7). The lines and line shapes in the high field and low field regions are consistent with rhombic *g*-values. There are about 10 lines in the center of the spectrum, which comprise the g_{mid} region. Assuming more than seven lines in the g_{mid} region, a seven line pattern for Cu(1.5)Cu(1.5) does not fit the experimental spectrum. Thus superhyperfine lines are observed involving splittings from, presumably, the bridging nitrogens. Using EPR parameters from Q-, X-, and S-band spectra, a simulation with g_{max}, g_{mid}, and g_{min} equal to 2.069, 2.066, and 2.00; A^{Cu} values of 44 G, 17 G, and 5 G; A^N values of 12 G, 17 G, and 5 G; fits the experimental spectrum extremely well (Figure 7). While simulations are consistent with, not proof of, the EPR parameters, the EPR experimental and simulated parameters do appear to be very close. One criterion for the goodness of fit is to simulate at another frequency without changing the EPR parameters. The simulation of the S-band spectrum is equally good, thus increasing the confidence in the EPR parameters (Supplemental Figure 4).

Discussion

Asymmetry in the coordination environment of the copper centers for $\{(^tBu_2\text{-}PNP)Cu\}_2^+$ and $\{(^tBu_2\text{-}PNP)Cu\}_2^{2+}$ has been observed via solid-state XRD analysis and is presumably a phenomenon specific to the solid-state.[xvii] This phenomenon was not observed for the (SNS)- and (PPP)-supported systems. For completeness, and direct comparison to the EPR data presented here, the solid-state X-ray structure of $\{(PNP)Cu\}_2^+$ has also been determined and placed in the Supporting Information. It likewise shows substantial asymmetry about the diamond core motif. In solution or upon freezing to a glass, however, $\{(PNP)Cu\}_2^+$ is a fully-delocalized, class-III mixed valence species based upon the EPR data available.

Cu_A has *g*-values of $g_{min} = 2.007$, $g_{mid} = 2.024$, and $g_{max} = 2.180$ (Table 1).[xxiv] For Cu_A, $g_{max} > g_{mid} \sim g_{min}$ and the ground state for the coppers is primarily $dx^2\text{-}y^2$. A *g*-value close to 2.00 for Cu_A suggests admixture of a low-lying excited state. This unusual behavior is also evident in our model compounds. For $\{(SNS)Cu\}_2^+$, $g_{min} = 2.00$, $g_{mid} = 2.066$, and $g_{max} = 2.069$. The ground state for the coppers involves the dz^2 orbitals more than the $dx^2\text{-}y^2$ orbitals as reflected by $g_l > g_{ll}$ where g_{mid} and g_{max} are g_l. For $\{(PNP)Cu\}_2^+$, $g_{min} = 2.00$, $g_{mid} = 2.055$, and $g_{max} = \sim 2.08$. Here the *g*-values are rhombic. In contrast, for $\{(PPP)Cu\}_2^+$, only one g-value from the crossover point, 2.003, is assigned as the signal is nearly isotropic at the resolutions we have achieved.

The line widths of the spectra in Figure 2 are consistent with sharp lines for $\{(SNS)Cu\}_2^+$, which have only copper and nitrogen hyperfine lines. For $\{(PNP)Cu\}_2^+$, the hyperfine lines are broader, consistent with an additional superhyperfine contribution from non-bridging

phosphorus. A key feature for the spectrum of $\{(PPP)Cu\}_2^+$ is the increase in the number of hyperfine lines, which are assigned to copper and bridging phosphorous atoms, where an increase in line width accounts for terminal phosphorous atoms.

The interpretation of the hyperfine and superhyperfine structure is simplest for $\{(SNS)Cu\}_2^+$ because there are no superhyperfine couplings from the terminal ligands. The lowest field lines in the spectrum (Figure 7) are separated from the other lines, equivalent to lines expected in a single crystal, and well simulated with $g_{max} = 2.069$, $A^{Cu}_{max} = 44$ G, and $A^{N}_{max} = 12$ G. The *g*- and *A*-tensors in the simulation are coincident, but it is not known how sensitive the spectra are to the Euler angles. The number of lines in the g_{mid} region is similar in both the experimental g_{mid} region and the simulated spectrum (Figure 7). It is concluded that there are more than seven lines in the g_{mid} region, which implies hyperfine lines from both copper and nitrogen. A crude simulation assuming a seven-line pattern for equivalent coppers has been published**Error! Bookmark not defined.21** but does not fit nearly as well as the simulation shown in Figure 7. The shape of the lines for g_{min} in the high field region are not as close to the experimental spectrum as for the lines in the g_{max} and g_{mid} region, but, other than the line width being narrow, little information about the parameters was gained from the experimental spectrum (Figure 7). Simulation parameters for the g_{min} region are $g_{min} = 2.00$, $A^{Cu}_{min} = 5$ G, and $A^{N}_{min} = 5$ G. A^{Cu}_{min} and A^{N}_{min} are much less than the parameters for A_{max} and A_{mid}, and hence the tensors are anisotropic. A^N for a terminal nitrogen is expected to be more isotropic. The anisotropic values for A^N for $\{(SNS)Cu\}_2^+$ and $\{(PNP)Cu\}_2^+$ thus appear to be characteristic for the bridging N-atoms. The isotropic values for $A^{P(bridging)}$ for $\{(PPP)Cu\}_2^+$ are approximate values because the *g*-values are quenched, making assignments for the x, y, and z directions more difficult and because the time to simulate with anisotropic values was prohibitive. Therefore the degree of anisotropy for $A^{P(bridging)}$ for $\{(PPP)Cu\}_2^+$ was not determined. Curiously, despite greater calculated Cu spin density in Cu_A relative to the $\{(LXL)Cu\}_2^+$ model compounds (Table 2), the values for A^{Cu} are more or less similar to the values for A^{CuA}, with A^{Cu} for $\{(PPP)Cu\}_2^+$ somewhat greater than for A^{CuA} and with A^{Cu} for $\{(PNP)Cu\}_2^+$ and $\{(SNS)Cu\}_2^+$ about the same or less than for A^{CuA}. It may be that the value for A (Cu) for $\{(PPP)Cu\}_2^+$ is not isotropic, but anisotropic and the anisotropy in the EPR spectrum is not readily evident. Under this case the spin density for Cu would be overestimated.

Recently XAS and electronic structure calculations were obtained for $\{(PNP)Cu\}_2^{n+}$ (n = 0,1,2) and $\{(PPP)Cu\}_2^{n+}$.[xvii] Rhee and Head-Gordon have independently undertaken a theoretical study of $\{(PPP)Cu\}_2^{n+}$.[xxv] It has been generally concluded that the redox chemistry for $\{(PPP)Cu\}_2^{n+}$ and $\{(^tBu_2\text{-}PNP)Cu\}_2^{n+}$ is substantially delocalized throughout the $Cu_2(\mu\text{-}XR_2)_2$ cores, with a majority component of the redox chemistry occurring at the bridging N or P units (Table 2). The values obtained for A^N and $A^{P(bridging)}$ are consistent with this hypothesis. Values from Table 1 for $A^{P(terminal)}$ for $\{(PPP)Cu\}_2^+$ of 12.5 G and for $\{(PNP)Cu\}_2^+$ of about 5 G are in accord with modest terminal phosphorous contributions. $A^{N(terminal)}$ is 5.6 G for Cu_A (Table 1), but the ratio of the nuclear moments for P to N is 2.26320 to 0.4037607. If the electron density for the terminal N and phosphorous were similar, a value of about 30 G would be expected for $A^{P(terminal)}$. The electron density on the bridging phosphorous or nitrogen is substantially greater (Table 1) than for the terminal phosphorous, which is in accordance with a large bridging atom *A* values. Moreover, quenching of the *g*-values for $\{(PPP)Cu\}_2^+$ to an almost isotropic value, together with delocalization of spin density on the bridging phosphorous, suggest the presence of P-centered radical character. A^N values for $\{(PNP)Cu\}_2^+$ and $\{(SNS)Cu\}_2^+$ (Table 1) are comparable to those observed for N-localized radicals such as Me_2N ($A^N = 14.7$ G)[xxvi] and nitroxide radicals (A^N approx 32 G).[xxvii] P-centered radicals are less common, and A^P values range from 42.5 G in highly delocalized systems[xxviii] to 96.3 G in $P[CH(SiMe_3)_2]_2$.[xxix] The *A* value in $\{(PPP)Cu\}_2$ (45 G) is in the range expected for free P-centered radicals. Such direct observation of $A^{X(bridging)}$ in

the $Cu_2(\mu\text{-}X)_2$ core of Cu_A is not possible because the bridging S atoms are spin inactive (I = 0).

Supplementary Material

Refer to Web version on PubMed Central for supplementary material.

Acknowledgement

JCP acknowledges support from the NSF (GOALI). NPM is grateful for an NSF graduate fellowship. WEA acknowledges the National Biomedical EPR Center Grant EB001980 from NIH. The authors are grateful to a reviewer for a helpful suggestion.

References

i. (a) Ambundo EA, Yu Q, Ochrymowycz LA, Rorabacher DB. Inorg. Chem 2003;42:5267. [PubMed: 12924898] (b) Kyritsis P, Dennison C, Ingeldew WJ, McFarlane W, Sykes AG. Inorg. Chem 1995;34:5370. (c) Groenveld CM, Canters GW. J. Biol. Chem 1988;263:167. [PubMed: 3121606] (c) Groenveld CM, Dahlin S, Reinhammer B, Canters GW. J. Am. Chem. Soc 1987;109:3247.

ii. (a) Solomon EI, LaCroix LB, Randall DW. Pure Appl. Chem 1998;70:799. (b) Randall DW, Gamelin DR, LaCroix LB, Solomon EI. J. Biol. Inorg. Chem 2000;5:16. [PubMed: 10766432]

iii. (a) Guss JM, Freeman HC. J. Mol. Biol 1983;169:521. [PubMed: 6620385] (b) Gray HB, Malmstrom BG, Williams RJP. J. Biol. Inorg. Chem 2000;5:551. [PubMed: 11085645]

iv. Shibata N, Inoue T, Nagano C, Nishio N, Kohzuma T, Onodera K, Yoshizaki F, Sugimura Y, Kai Y. J. Biol. Chem 1999;274:4225. [PubMed: 9933621]

v. Suzuki S, Kataoka K, Yamaguchi K, Inoue T, Kai Y. Coord. Chem. Rev 1999;192:245.

vi. Marcus RA, Sutin N. Biochim. Biophys. Acta 1985;811:265.

vii. (a) Houser RP, Young VG Jr. Tolman WB. J. Am. Chem. Soc 1996;118:2101. (b) Blackburn NJ, deVries S, Barr ME, Houser RP, Tolman WB, Sanders D, Fee JA. J. Am. Chem. Soc 1997;119:6135. (c) Hagadorn JR, Zahn TI, Que L Jr. Tolman WB. J. C. S. Dalton Trans 2003:1790.

viii. Al-Obaidi A, Baranovič G, Coyle J, Coates CG, McGarvey JJ, McKee V, Nelson J. Inorg. Chem 1998;37:3567. [PubMed: 11670445]

ix. (a) LeCloux DD, Davydov R, Lippard SJ. Inorg. Chem 1998;37:6814. [PubMed: 11670817] (b) LeCloux DD, Davydov R, Lippard SJ. J. Am. Chem. Soc 1998;120:6810. (c) He C, Lippard SJ. Inorg. Chem 2000;39:5225. [PubMed: 11154580]

x. Gupta R, Zhang ZH, Powell D, Hendrich MP, Borovik AS. Inorg. Chem 2002;41:5100. [PubMed: 12354043]

xi. Vallee BL, Williams RJP. Proc. Nat. Acad. Sci. U.S.A 1968;59:498.

xii. Rorabacher DB. Chem. Rev 2004;104:651. [PubMed: 14871138]

xiii. (a) Gamelin DR, Randall DW, Hay MT, Houser RP, Mulder TC, Canters GW, de Vries S, Tolman WB, Lu Y, Solomon EI. J. Am. Chem. Soc 1998;120:5246. (b) George SD, Metz M, Szilagyi RK, Wang HX, Cramer SP, Lu Y, Tolman WB, Hedman B, Hodgson KO, Solomon EI. J. Am. Chem. Soc 2001;123:5757. [PubMed: 11403610] (c) Szilagyi RK, Lim BS, Glaser T, Holm RH, Hedman B, Hodgson KO, Solomon EI. J. Am. Chem. Soc 2003;125:9158. [PubMed: 15369373]

xiv. Harkins SB, Peters JC. J. Am. Chem. Soc 2004;126:2885. [PubMed: 14995206]

xv. Mankad NP, Rivard E, Harkins SB, Peters JC. J. Am. Chem. Soc 2005;127:16032. [PubMed: 16287283]

xvi. Harkins SB, Peters JC. J. Am. Chem. Soc 2005;127:2030. [PubMed: 15713065]

xvii. Harkins SB, Mankad NP, Miller AJM, Szilagyi RK, Peters JC. J. Am. Chem. Soc 2008;130:3478. [PubMed: 18298114]

xviii. Froncisz W, Hyde JS. J. Magn. Reson 1982;47:515.

xix. Hyde JS, Newton ME, Strangeway RA, Camenisch TG, Froncisz W. Rev. Sci. Instrum 1991;62:2969.

xx. The experimental X-band EPR spectrum of {(PNP)Cu} $^{+}_{2}$ has not been previously published. The experimental X-band spectrum of {(SNS)Cu} $^{+}_{2}$ can be found in reference xiv, and that for {(PPP)Cu} $^{+}_{2}$ can be found in the Supporting Information of reference xv.

xxi. (a) Sjoberg B-M, Peichard P, Graslund A, Ehrenberg A. J. Biol. Chem 1977;252:536. [PubMed: 188819] (b) Graslund A, Sahlin M, Sjoberg B-M. Environ. Health Perspect 1985;64:139. [PubMed: 3007085]

xxii. Barr ME, Smith PH, Antholine WE, Spencer B. J. Chem. Soc. Chem. Commun 1993:1649.

xxiii. Kababya S, Nelson J, Calle C, Neese F, Goldfarb G. J. Am. Chem. Soc 2006;128:2017. [PubMed: 16464103]

xxiv. Neese F, Zumft WG, Antholine WE, Kroneck PMH. J. Am. Chem. Soc 1996;118:8692.

xxv. Rhee YM, Head-Gordon M. J. Am. Chem. Soc 2008;130:3878. [PubMed: 18314976]

xxvi. Brand JC, Cook MD, Roberts BP. J. Chem. Soc., Perkin Trans. II 1984:1187.

xxvii. Libertint LJ, Griffith OH. J. Chem. Phys 1970;53:1359.

xxviii. Agarwal P, Piro NA, Meyer K, Müller P, Cummins CC. Angew. Chem., Int. Ed 2007;46:3111.

xxix. Gyanne MJS, Hudson A, Lappert MF, Power PP, Goldwhite H. J. Chem. Soc., Dalton Trans 1980:2428.

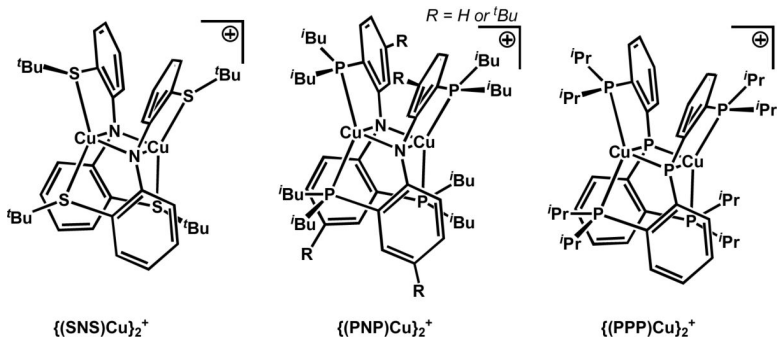

Figure 1.
$Cu_2(\mu\text{-}XR_2)_2$ diamond core systems featured in the present study.

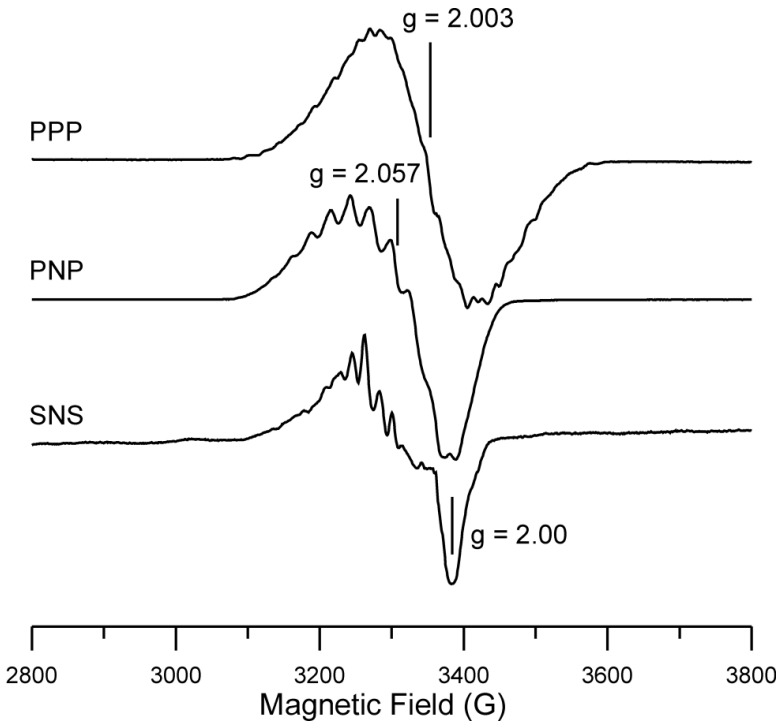

Figure 2.
X-band EPR spectra of $\{(PPP)Cu\}_2^+$, $\{(PNP)Cu\}_2^+$, and $\{(SNS)Cu\}_2^+$

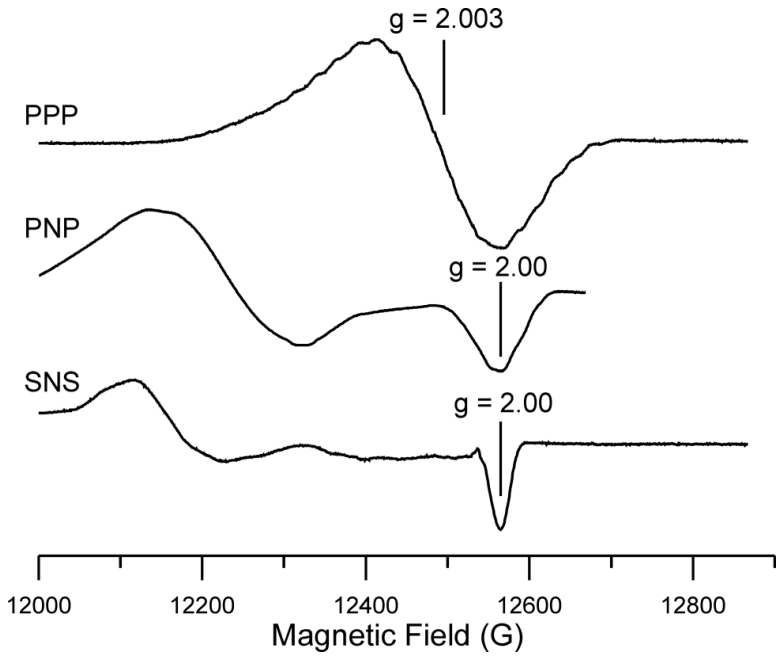

Figure 3.
Q-band EPR spectra of $\{(PPP)Cu\}_2^+$, $\{(PNP)Cu\}_2^+$, and $\{(SNS)Cu\}_2^+$

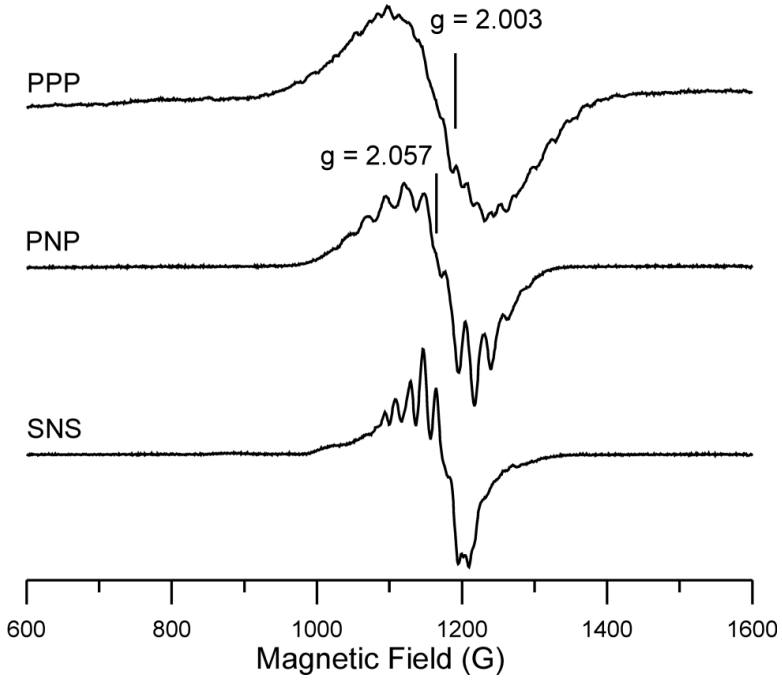

Figure 4.
S-band EPR spectra of $\{(PPP)Cu\}_2^+$, $\{(PNP)Cu\}_2^+$, and $\{(SNS)Cu\}_2^+$

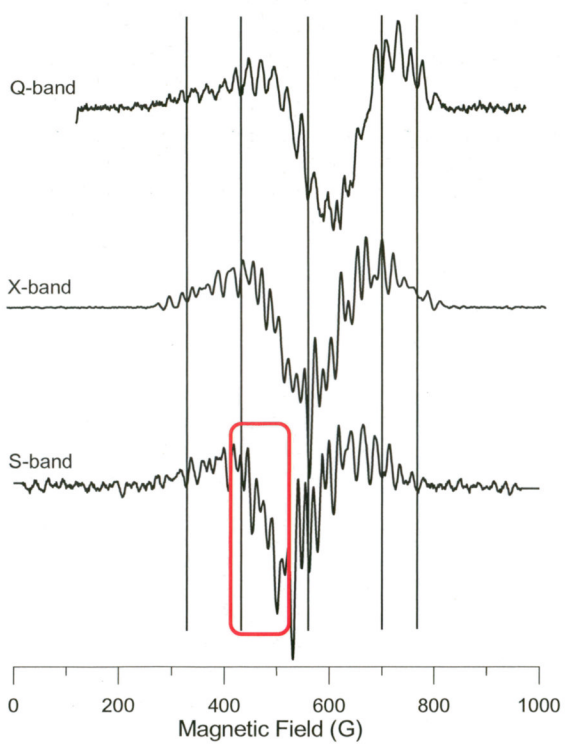

Figure 5.
Second derivative of Q-, X-, and S-band spectra for $\{(PPP)Cu\}_2^+$

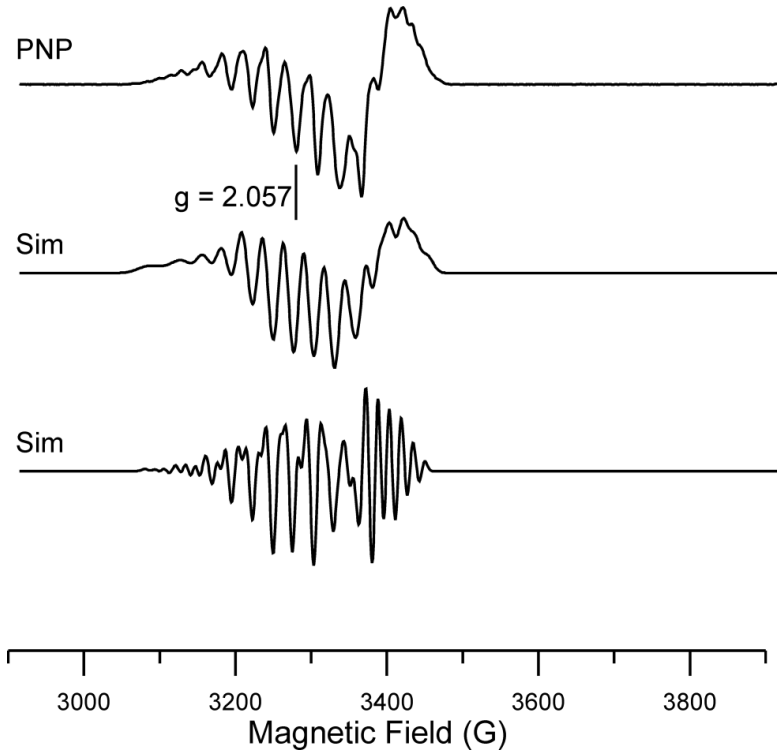

Figure 6.

Second derivative X-band spectrum for $\{(PNP)Cu\}_2^+$ and simulations. EPR parameters for simulations: g_{max}, g_{mid}, g_{min}, 2.085, 2.057, 2.000; A^{Cu}_{max}, A^{Cu}_{mid}, A^{Cu}_{min}, 40, 27, 15 G; A^{N}_{max}, A^{N}_{mid}, A^{N}_{min}, 12, 24, 15 G; line width 15, 11, 10 G (top simulation), 5, 5, 5 G (bottom simulation); microwave frequency, 9.434 GHz.

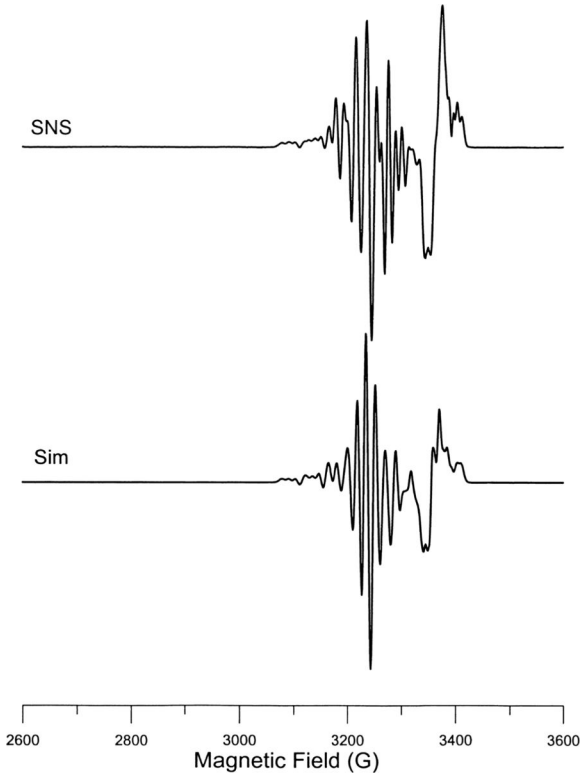

Figure 7.

Second derivative X-band spectrum for {(SNS)Cu}$^{+}{}_{2}$ and simulation. EPR parameters for simulation: g_{max}, g_{mid}, g_{min}, 2.069, 2.066, 2.00; $A^{Cu}{}_{max}$, $A^{Cu}{}_{mid}$, $A^{Cu}{}_{min}$, 44, 17, 5 G; $A^{N}{}_{max}$, $A^{N}{}_{mid}$, $A^{N}{}_{min}$, 12, 17, 5 G; line width 7, 7, 4 G; microwave frequency, 9.377 GHz.

Table 1

EPR parameters for $\{(LXL)Cu\}_2^+$ from simulations, and comparative literature values for Cu_A and the mixed-valence complex $Cu_2L^{\#}$.

	g_{max}	g_{mid}	g_{min}	A_{max}^{Cu}	A_{mid}^{Cu}	A_{min}^{Cu}	A_{max}°	A_{mid}°	A_{min}°	A'
$\{(PPP)Cu\}_2^+$	---	2.00	---	---	45 G	---	---	45 G	---	12.5 G
$\{(PNP)Cu\}_2^+$	2.08	2.06	2.00	~40 G	27 G	15 G	~12 G	24 G	15 G	~5 G
$\{(SNS)Cu\}_2^+$	2.07	2.06	2.00	~44 G	17 G	~5 G	~12 G	17 G	~5 G	---
Cu_A	2.180	2.024	2.007	40 G	21 G	21 G	---	---	---	5.6 G
Cu_2L	2.15	2.15	2.02	103 G	103 G	21 G	---	---	---	5-9 G

*EPR parameters for A^{Cu} for Cu_A corrected for ^{63}Cu instead of ^{65}Cu as given in the ref. 5. Values were averaged for $A^{Cu(1)}$ and $A^{Cu(2)}$ for Cu_A.

**An isotropic g-value for PPP is assumed. The g-value is taken as the crossover point in the Q-band spectrum, but the crossover point moves to 2.014 at X-band and 2.055 at S-band. A marker for $g = 2.003$ is evident in Figs. 2, 3, and 4. Since g_{min} and g_{mid} are not resolved in the Q-band spectrum, an error of ± 0.02 is assumed.

***g-values were calibrated using DPPH. For g_{min}, the high field sharp line in the spectra for SNS, the calculated g-values are 2.001 for S-band, 1.998 for X-band, and 1.990 for Q-band. The g_{min} for SNS is set to 2.00 ± 0.01.

°This hyperfine value is attributed to the bridging N or P atom.

‘This superhyperfine value is attributed to the non-bridging P or N donor.

#L is $(N[CH_2CH_2N(H)CH_2CH_2N(H)CH_2CH_2]_3N)$, ref xxii; $A^{N'}$ taken from ref xxiii.

Table 2

Estimated spin density distribution from DFT calculations.

Cu_A [xxiv]	38% Cu	44% bridging S		
$\{(PPP)Cu\}_2^+$ [xvii]	18% Cu	44% bridging P	14% terminal P	22% C and H
$\{(^tBu\text{-}PNP)Cu\}_2^+$ [xvii]	16% Cu	35% bridging N	11% terminal P	38% C and H